2007

Performance quantification of conducting polymer actuators for real applications: a microgripping system

Gursel Alici
University of Wollongong, gursel@uow.edu.au

Nam N. Huynh
University of Wollongong, nhuynh@uow.edu.au

Publication Details

Alici, G. & Huynh, N. (2007). Performance quantification of conducting polymer actuators for real applications: a microgripping system. IEEE - ASME Transactions on Mechatronics, 12 (1), 73-84.

Performance Quantification of Conducting Polymer Actuators for Real Applications: A Microgripping System

Gursel Alici and Nam N. Huynh

***Abstract*—In this paper, we report on modeling, characterization, and performance quantification of a conducting polymer actuator, driving a rigid link to form each finger of a two-finger gripping system, which is what we call a microgripping system. The actuator, which consists of five layers of three different materials, operates in a nonaquatic medium, i.e., air, as opposed to its predecessors. After the bending displacement and force outputs of a single finger are modeled and characterized including the effect of the magnitude and frequency of input voltages, the nonlinear behavior of the finger including hysteresis and creep effects is experimentally quantified, and then a viscoeleastic model is employed to predict the creep behavior. The experimental and theoretical results presented demonstrate that while the hysteresis is negligibly small, the creep is significant enough so as not to be ignored. The response of the actuator and the finger under step input voltages is evaluated, and found that the actuator does not have any time delay, but only a large time constant. Two of the fingers are assembled to form a microgripping system, whose payload handling and positioning ability has been experimentally evaluated. It can lift up to 50 times its weight under 1.5 V. The payload handled was a spherical object covered with industrial type tissue paper. The friction coefficient between the object and the carbon fiber rigid link has been determined experimentally and used to estimate the contact force. All the theoretical and experimental performance quantification results presented demonstrate that conducting polymer actuators can be employed to make functional microsized robotic devices.**

***Index Terms*—Actuators, electroactive polymer actuators, flexure-based devices, micromanipulation, system identification/characterisation.**

I. Introduction

As POTENTIAL electromechanical actuators and sensors, which are very suitable for miniaturization, conducting polymer actuators have attracted the attention of many researchers in the last decade [1]–[9]. A comprehensive account of polymer actuators is given in [1] and [9]. They have a composite structure with polymer layers separated from each other with an insulator. When the right stimulus, which is usually a very small voltage, typically 1 V or a current, is applied to the polymer layers, a volume expansion and contraction occurs due to electrochemomechanical properties of the polymers [10]–[12]. The change in the volume generates a bending displacement—the electrochemical energy is converted into mechanical energy. As a result, considerable amount of research has been devoted to modeling and understanding their behavior in order to improve their synthesis conditions for use as reliable actuators and sensors for new cutting applications ranging from biomedical devices to micromanipulators [4] [7] [13]. Zhou *et al*. [4] have reported on three types of polymer actuators including ionic conducting polymer film actuator, polyaniline actuator, and parylene thermal actuator. They have presented their fabrication and initial performance results. Zhou and Li [14] have reported on the MEMS-based fabrication of cantilever microstructures consisting of Au/Nafion/Au trilayers on silicon substrates in order to construct microgrippers operating in aqueous media. Smela *et al*. [7] have presented the development and performance outcomes of polypyrrole (PPy) and Au bilayer conducting polymer actuators *operating in electrolyte solutions*. As an extension of this study, Jager *et al*. [13] have fabricated a serially connected micromanipulator to pick, move, and place 100-μm glass beads.

This paper is part of an ongoing-project on the establishment of manipulation systems such as grippers and planar mechanisms, articulated with the fourth generation PPy actuators fabricated in the Intelligent Polymer Research Institute at the University of Wollongong [2]. Conducting polymers have many promising features including low actuation voltage, operation in aquatic mediums and in air, low cost, and high force–output weight ratio. Their main drawback is their low speed of response and nonlinearity due to the actuation principle, which is based on mass transfer. The application of conducting polymer actuators is an emerging field, as researchers begin to harness the benefits of their material properties, which are greatly enhanced at smaller scales [9]. Possible future applications include artificial muscles and a wide variety of sensors and actuators in biomedical systems [6] and micro/nano manipulation systems [15]. As these actuators do not contain any rolling and sliding elements, they are suitable for micro/nano manipulation tasks, which require motion accuracy of the order of 0.05–0.1 μm (50–100 nm). In our previous studies [16]–[20], we reported on developing various mathematical models to predict the bending behavior of the conducting polymer actuators, and employing the models to optimize their topology with high force and displacement outputs.

In this paper, we report on the performance quantification of a PPy-based conducting polymer actuator driving a rigid

Manuscript received November 20, 2005; revised April 26, 2006. Recommended by Technical Editor J. P. Desai. This work was funded in part by a University Research Council (URC) grant.

G. Alici is with the School of Mechanical, Materials and Mechatronic Engineering, and the ARC Center of Excellence on Electromaterials Science, University of Wollongong, NSW 2522, Australia (e-mail: gursel@uow.edu.au).

N. N. Huynh is with the School of Mechanical, Materials and Mechatronic Engineering, University of Wollongong, NSW 2522, Australia (e-mail: nnh275@uow.edu.au).

Digital Object Identifier 10.1109/TMECH.2007.886256

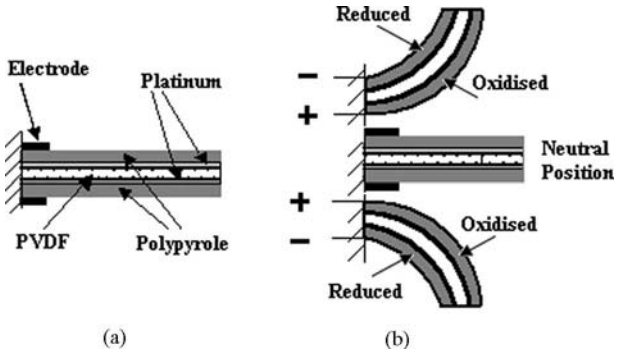

Fig. 1. (a) Schematic structure of the conducting polymer actuator. (b) Schematic representation of the bending principle.

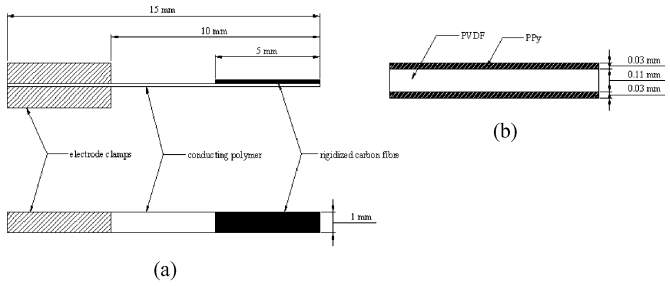

Fig. 2. Structure and dimensions of the robotic finger. (a) Front view and top view. (b) Cross section of the actuator part (not to scale).

carbon fiber link, which constitutes each finger of a microgripping system with the dimensions of (5-mm actuator + 5-mm rigid link) × 1 mm × 0.17 mm. With reference to these dimensions and its fabrication process, the microgripping system is not MEMS-based. It must be noted that surface micromachining, bulk micromachining (i.e., etching), bonding alone, electrodeposition, photolithography, and other replication techniques are used to make MEMS-based microdevices/microstructures. The performance evaluation has been realised in terms of the bending displacement and force output, and their nonlinear behavior including hysteresis and creep. The actuator has been used in a real application to articulate a two-finger gripper. The experimental and estimated results attest that electroactive polymer actuators are suitable to make micromanipulation devices such as a gripper, which can handle as much as 50 times its total mass.

II. Polymer Actuator Driving a Rigid Link

The polymer actuator and the rigid link form a monolithic composite structure, where the polymer section serves as the actuator and a flexure joint—like an active flexure joint, and the rigid link as a payload carried by the actuator.

A. Actuation Structure and Mechanism

The structure of the PPy-based polymer actuator, considered in this paper, is shown in Fig. 1. The actuator has five layers. The outer two layers, which are PPy with thicknesses of 30 μm, are the electroactive elements providing actuation. The middle layer is polyvinylidine fluoride (PVDF), an inert, nonconductive, porous polymer. It serves as a separator for the two PPy layers and the reservoir for electrolyte (tetrabutylammonium hexafluorophosphate) TBA PF_6 0.05 M in solvent propylene carbonate. The electrolyte and the solvent need to be stored in the PVDF layer in order to operate the actuator in air. Otherwise, it has to be operated in an aqueous medium consisting of the electrolyte and the solvent. Thin layers of platinum of 10–100 Å are sputter-coated on both sides of PVDF to enhance the conductivity between the PPy layers and the electrolyte. When an electrical potential is applied across the electrodes attached to the PPy layers, the reduction/oxidation (redox) process occurs, and the actuator bends. For the actuator employed in this study, the redox process is described by

$$\underset{\text{(oxidation state)}}{PPy^{+}PF_6^{-}+e^{-}} \overset{\text{oxidation reduction}}{\longleftrightarrow} \underset{\text{(reduced state)}}{PPy^{0}+PF_6^{-}}. \quad (1)$$

The redox process occurs simultaneously on both the PPy layers; while one layer is oxidized, the other is reduced, and vice versa. With reference to (1), the displacement of PF_6^- ions in the PPy layers causes material strain through a number of effects. One is the effect of the gain or loss of ion volume causing volume expansion or contraction in the PPy layers. The movement of solvent molecules due to osmotic pressure, which accompany the ion diffusion, also contributes to the volume change in the PPy layers. The other factor is the resultant electrostatic forces between the displaced ions and the polymer backbone that cause the PPy layers to expand or contract. As the two PPy layers undergo opposing strains, a bending moment is induced, generating the deflection of the actuator.

B. Robotic Finger

The structure of the robotic finger made up of the polymer actuator and carbon fiber is shown in Fig. 2.

The conducting polymer part of the finger works as an actuator and a flexure joint called *active flexure (acti-flex)* joint, while the carbon fiber attached to the end of the polymer serves as a rigid link for the robotic finger.

The finger is fabricated as follows.

- An already fabricated sheet of conducting polymer is trimmed into strips of 1 mm × 15 mm, and the carbon fiber with a thickness of 0.3 mm is trimmed into pieces of 1 mm × 5 mm.
- The carbon fiber pieces are cured in an oven for about 10 min at 100 °C to make it rigid.
- A double-sided sticky tape is put onto the rigid carbon fiber pieces.
- The rigid carbon fiber pieces with the sticky tape on one side are then attached to the polymer strip to make the finger.
- The samples are replenished in TBA PF_6 0.05-M electrolyte for 5 min before each test.

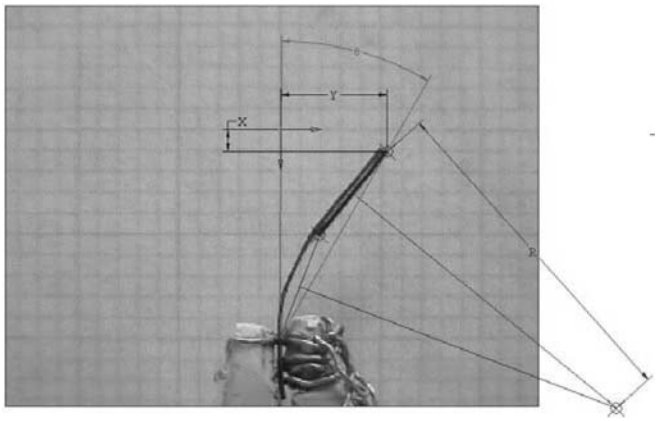

Fig. 3. Parameters defining the finger tip position: coordinate systems, bending angle, and the radius of curvature. The radius was measured from the intersection of the perpendicular lines of two adjacent segments.

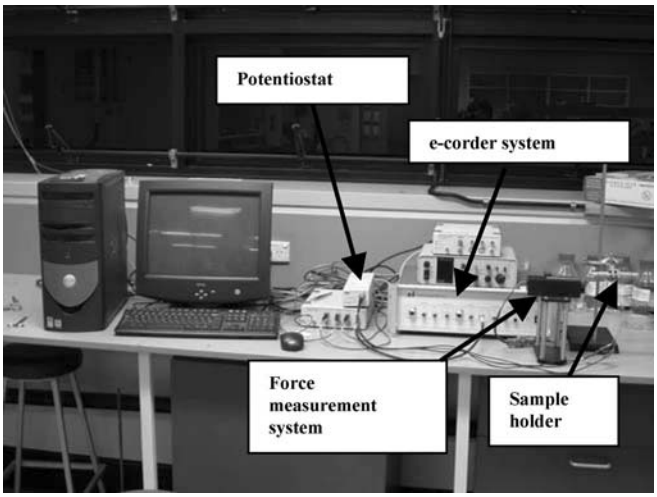

Fig. 4. Experimental setup.

III. Experimental Performance Quantification of Robotic Finger

The fabricated finger has the dimensions of (5-mm actuator + 5-mm rigid link) × 1 mm × 0.17 mm, as depicted in Fig. 3. A photograph of all the apparatus used for experiments is shown in Fig. 4. eDAQ e-corder recorder unit together with eDAQ Chart and eDAQ Scope software is used to record, amplify, filter, and analyse data. Aurora Scientific Inc. dual-mode lever arm system, model 300 B is used to measure the tip force. The platinum wires on the electrode clamps are connected to the outputs of a potentiostat/galvanostat, controlled using Chart 4 Windows software via a Powerlab 4/20 controller. Other equipments include a PC, a digital video camera, a metal stand and clamps, two-electrode clamps and a grid paper. The schematic representation of the experimental setup employed to evaluate the performance of the finger is shown in Fig. 5.

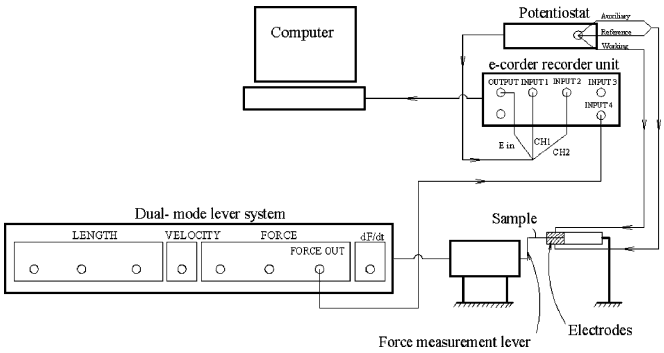

Fig. 5. Schematic representation of the equipment.

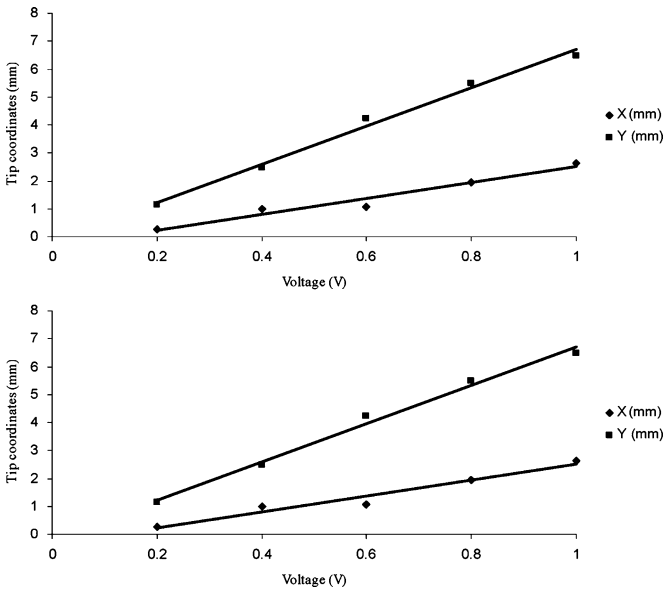

Fig. 6. Tip displacements for two equivalent robotic fingers under a range of constant input voltages.

A. Effect of Input Voltages on Displacement Output of a Robotic Finger

Under constant voltages ranging from 0.2 to 1 V, the tip displacements of the robotic finger is measured, and are shown in Fig. 6 for two samples of the same finger. The same experiments, which were conducted for the polymer actuator with the dimensions of 5 mm × 1 mm × 0.17 mm, had shown the same trends, i.e., the higher the input voltage, the larger the tip displacement. However, it must be noted that the displacement along the x-axis is much smaller than the displacement along the y-axis. In Section IV, a mathematical model to predict the bending displacement of the actuator is presented. It must be noted that the corresponding radii of curvature depicted in Fig. 7 are needed for the force model provided in the next section. The tip displacement results of our trilayer actuator operating in air is in agreement with the performance characterisation results presented in the literature for a trilayer polymer actuator (20 mm × 15 mm × 0.013 mm) operating in a 1-M $LiClO_4$ aqueous solution under current control [12].

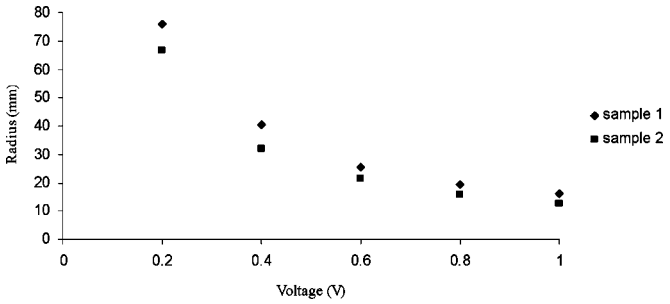

Fig. 7. Measured radii of curvature for two equivalent robotic fingers under a range of constant input voltages.

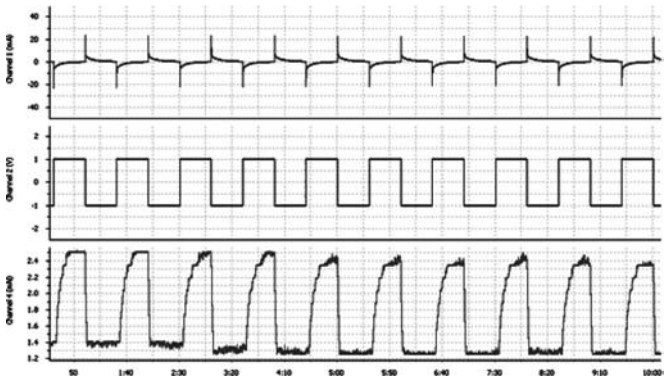

Fig. 8. Experiment data recorded under a square wave with a magnitude of $\pm$ 1 V with the frequency of 1 PPM.

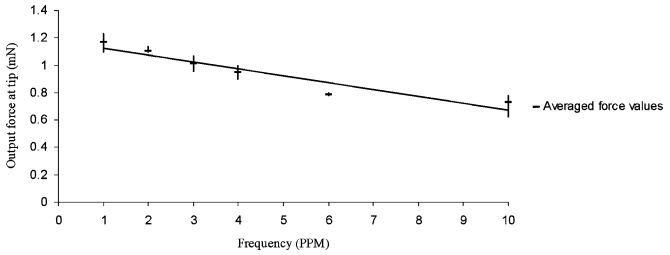

Fig. 9. Variation of the output force with input frequency.

B. Effect of Frequency of the Input Voltages on the Force Output of a Robotic Finger

The force output of the robotic finger is measured under a set of square waves with a constant magnitude of ± 1 V and the frequencies of 10 pulses/min (PPM) or 0.1667 Hz, 6 PPM or 0.1 Hz, 4 PPM or 0.0667 Hz, 3 PPM or 0.05 Hz, 2 PPM or 0.0333 Hz, and 1 PPM or 0.0167 Hz. Before each test, an input voltage of 0 V is applied to neutralize the finger. The current passed through the oxidized polymer layer, the input voltage, and the output force, data extracted from the eDAQ data logging system, are shown in the top, middle, and bottom plots of Fig. 8, respectively. These are typical data recorded for each frequency.

The magnitude of the force for each frequency is read from the recorded force data, and is shown in Fig. 9, where the force decreases linearly with the input frequency. This can be explained by the fact that the movement of dopant ions and solvent molecules requires certain time to move in and out of the PPy layers during the redox process. Obviously, with high input frequencies, there is not sufficient time for the ions and the molecules to reach deep into the polymer layer to generate more force. This is like stopping their movement in the middle of their journey and asking them to go back. This argument is supported by the magnitude of the minimum current passing through the oxidized layer, i.e., if the minimum current is closer to zero, the better will be the oxidation, which generates more actuation effect. The minimum current for the input frequencies is determined from the recorded current data, as shown in Fig. 10, where the magnitude of the minimum current under a relatively high input frequency is significantly higher than that of the low input frequency.

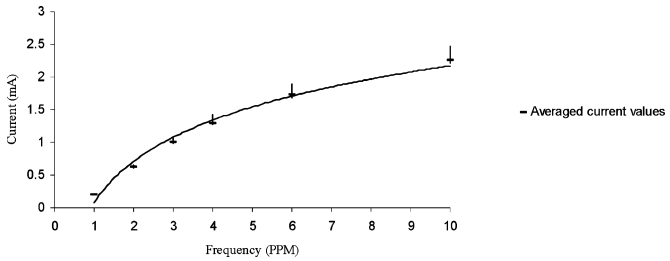

Fig. 10. Variation of the minimum current recorded during force measurement with the frequency.

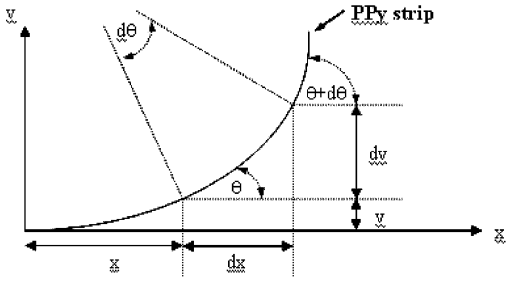

Fig. 11. Bending curve of a bending polymer actuator.

IV. Bending Motion and Bending Force Modeling

The mathematical models are needed to provide enhanced degrees of understanding, predictability, control, and efficiency in performance in order to improve the displacement and force outputs of the polymer actuators before using them in real applications [20].

A. Bending Motion Model

This mathematical model, which had been reported in our previous study [16], is summarized here for the sake of completeness. The model has been derived in terms of the tip vertical displacement v and the horizontal displacement x, as shown in Fig. 11.

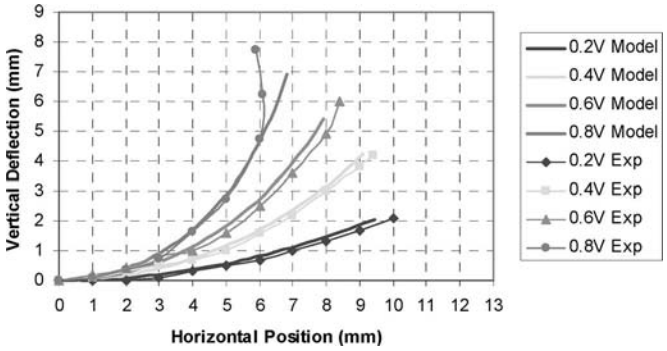

Fig. 12. Experimental and theoretical bending curves for a polymer actuator [dimensions: 10 mm × 1 mm × 0.21 mm; $\beta = 0.145$ (F/m^2)/(C/m^3)] [16].

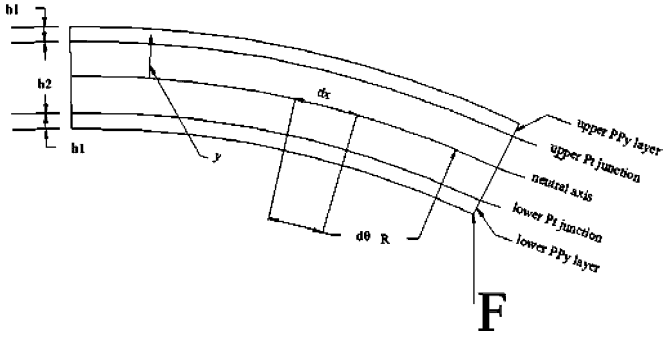

Fig. 13. One end cantilevered actuator and the parameters in the model.

The resulting mathematical model is a second-order nonlinear differential equation given by

$$\frac{d^2v}{dx^2} - \left[1 + \left(\frac{dv}{dx}\right)^2\right] \frac{3\beta VC(h_2 + h_1)}{2bL\left[E_1\left(\frac{2h_1+h_2}{2}\right)^3 + (E_2 - E_1)\left(\frac{h_2}{2}\right)^3\right]} = 0 \qquad (2)$$

where V is the input voltage, L is the length of the actuator, b is the width of the actuator, C is the capacitance, E_1 and E_2 are Young's moduli of PPy and PVDF layers, respectively, h_1 and h_2 are described in Fig. 13, and β is the experimentally determined proportionality constant relating the internal stress σ to the exchanged charge density given by

$$\sigma = \beta \frac{\Delta Q}{B} \qquad (3)$$

where ΔQ is the exchanged charge, and B is the volume of the oxidised PPy layer of the actuator. The model given by (2) has been solved for the dimensions and mechanical properties of the known actuators, and then compared to the experimental bending results under the voltage step inputs of 0.2, 0.4, 0.8, and 1.0 V, as depicted in Fig. 12. The theoretical results match the experimental results quite closely. It should be noted that the model does not account for bending beyond 90°, which is why the tips of the curves with larger deflections show the greatest discrepancy, while the rest of the actuator shows a better agreement [16].

B. Force Output Model

It must be noted that many of the modeling approaches reported in the literature [8], [21] are mainly for bilayer polymer strips, based on the bending modeling of a bimetal thermostat reported by Timoshenko [22]. In [19], the Timoshenko's method has been extended to model force outputs of the trilayer polymer actuator and the robotic finger. With reference to Fig. 13, the force F is the external force needed to block the bending displacement of the actuator tip. In fact, F is the force measured by the force sensor upon the activation of the polymer actuator. Under a quasistatic condition, the total moment consisting of the induced internal bending moment and the moment created by the external force F is always zero at any cross section along the actuator [19]

$$\Rightarrow \frac{1}{R}EI + \alpha E_1 b h_1 (h_1 + h_2) - FL = 0 \qquad (4)$$

where $EI = E_1 I_1 + E_2 I_2$ is the flexural rigidity of the whole actuator. It must be noted that the strain in the PPy layers at a distance y from the neutral axis due to the thickness change of the PPy layer during the redox process is constant throughout the PPy layers and is denoted by α. It is reported in the literature that α is a function of the strain-to-charge ratio and charge density in the PPy layers [16] [19].

Equation (4) describes two cases under a nonzero input voltage: 1) the tip of the actuator is not blocked (i.e., $F = 0$) and 2) the actuator tip is blocked to measure the tip force.

The first case is used to determine the value of α under different input voltages, provided that the radius of curvature R, and the numerical values of the other parameters in (4) are known. The radius of curvature is measured from the actuator bent under a nonzero input voltage, as given in Fig. 7

$$\alpha = -\frac{EI}{RE_1 b h_1 (h_1 + h_2)}. \qquad (5)$$

The calculated values of α are then employed to estimate the force produced at the actuator tip, from the second case:

$$F = \frac{E_1 b \alpha h_1 (h_1 + h_2)}{L}. \qquad (6)$$

In obtaining (6), we assume that the radius of curvature is extremely large $(1/R \approx 0)$. It can be inferred from (6) that the tip force is inversely proportional to the actuator. This follows that polymer actuators are also suitable for miniaturisation. The force model described by (6) can be applied to calculate the force at the tip of a robotic finger shown in Fig. 14. It is worth noting that the rigid part apparently does not contribute to the bending of the finger. The equivalent force F_{finger} acting at the tip of the rigid part is calculated from

$$F_{\text{finger}} = F\frac{L}{L'}. \qquad (7)$$

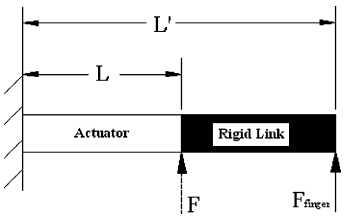

Fig. 14. Demonstration of parameters in the force model for the robotic finger.

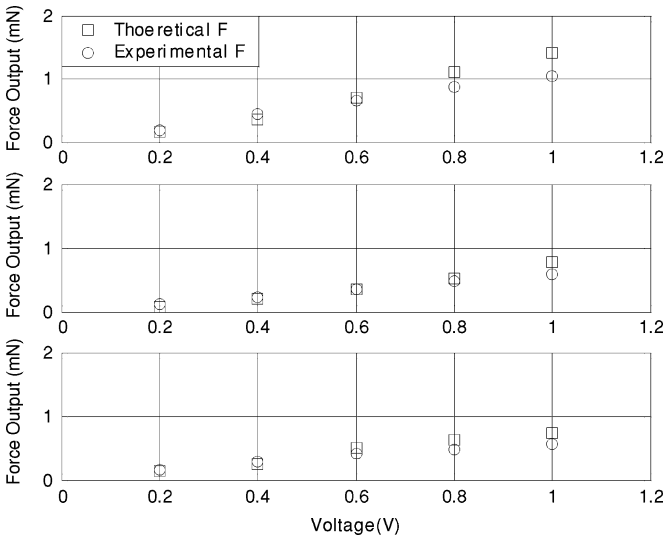

Fig. 15. Theoretical and experimental force results for the 5-mm actuator (*top plot*), the 10-mm actuator (*middle plot*), and the robotic finger (*bottom plot*).

V. Experimental Verification of Force Model

Step response experiments were carried out to verify the force models described by (6) and (7). The numerical values of the parameters in the force models [16] are:

1) PPy thickness $h_1 = 0.03$ mm;
2) PVDF thickness $h_2 = 0.11$ mm;
3) width of the finger $b = 1$ mm;
4) Young's modulus of PPy $E_1 = 80$ N/mm^2;
5) Young's modulus of PVDF $E_2 = 440$ N/mm^2.

To verify the force model of the bending actuator without the rigid link described by (6), two samples of the actuator with the dimensions of 5 mm $\times$ 1 mm $\times$ 0.17 mm and 10 mm $\times$ 1 mm $\times$ 0.17 mm are experimented with. Similarly, to verify the force model of the bending actuator with the rigid link described by (7), a robotic finger with the dimensions of $(5 + 5)$ mm $\times$ 1 mm $\times$ 0.17 mm is experimented with. The experimental and the predicted force results using (6) for the two actuators, and using (7) for the finger are shown in the top, middle, and bottom plots of Fig. 15, respectively. These results demonstrate that the force model is effective enough to predict the force outputs of the actuator without and with a rigid link quite well. To the best of our knowledge, this is the first study to establish an experimentally verified force model for a trilayer actuator operating in a nonliquid environment.

Experiments were also conducted to characterize the transient response of the 5 and 10 mm actuators, and of the robotic finger

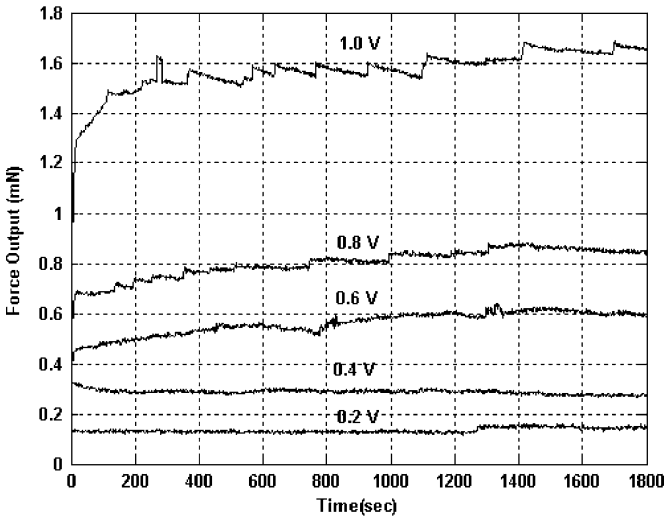

Fig. 16. Force response of the 5-mm actuator under step input voltages.

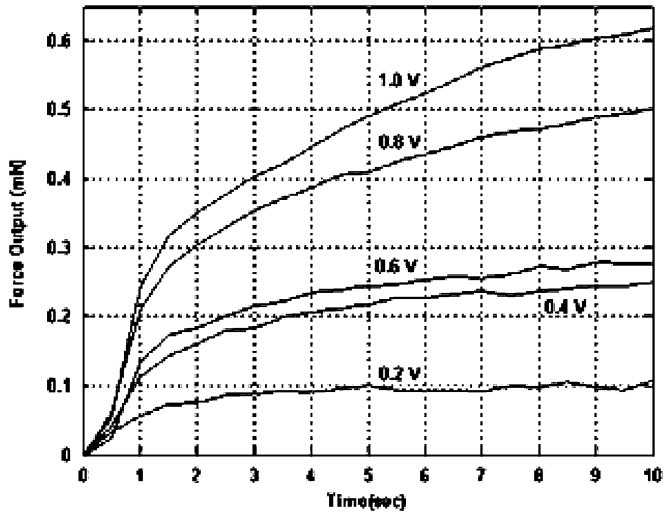

Fig. 17. Force responses of the 5-mm actuator in the first 10 s.

under a range of step voltages [19]. The results for the 5-mm actuator only are shown in Fig. 16 for the sake of brevity.

A closeup of the force responses of the 5-mm actuator in the first 10 s is shown in Fig. 17. It can be seen from these results that there is almost no initial delay (time delay) in the response of the actuator. A change in the force was recorded almost right after a change in the input voltage. However, the settling time is quite significant for voltage inputs to reach a steady-state value. Further, the results indicate that the actuator shows a capacitive response [5] [23] with a large time constant, which is one of the main disadvantages of electroactive polymer actuators. To circumvent this disadvantage, a new trilayer polymer actuator, which has been fabricated at our polymer research laboratory, has a time constant of as small as 0.47 s. These results of the time constants of the trilayer PPy actuators are better than those of the bilayer PPy actuators presented in the literature [6] [7], in which the response time was reported to be of the order of seconds. The synthesis and performance evaluation of the new faster actuators are reported in [24].

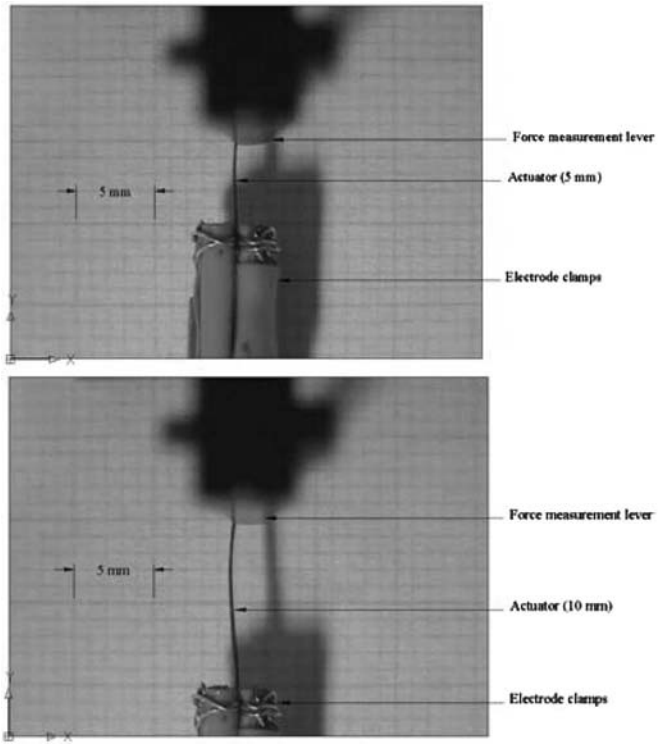

Fig. 18. 5-mm actuator (*top plot*) and 10-mm actuator (*bottom plot*) bending against the force measurement lever.

With reference to the results depicted in Fig. 15, there is quite a good agreement between the experimental and the predicted results with the input voltages up to 0.8 V for both actuator samples and up to 0.4 V for the robotic finger. This is due to the assumption of a negligibly small reciprocal of the radius of curvature $(1/R \approx 0)$ on which the force models, (6) and (7), are based. In fact, force measurement experiments showed that the curvature does exist when the actuator bends against the force measurement lever. Such bending is more obvious at higher input voltages and with longer actuators. This phenomenon is shown in Fig. 18 for the 10- and 5-mm actuators under step input voltages of 1.0 V, when bending against the force lever. It can be seen that the curvature of such bending is negligible for the 5-mm actuator, but quite obvious for the 10-mm actuator.

VI. Nonlinear Behavior of Actuator

Although polymer actuators have many positive features, they suffer from nonlinear problems such as hysteresis and creep, which deserve a comprehensive investigation. It must be kept in mind that, in the published literature, there are no experimental or theoretical results demonstrating the nonlinear behavior of trilayer polymer actuators operating in air.

A. Hysteresis Evaluation for the Robotic Finger

The input voltage in the form of a cyclic triangle signal is applied to the robotic finger operating in the horizontal plane. The movement of the actuator sample is recorded after one cycle and five working cycles by a digital video camera. The tip position

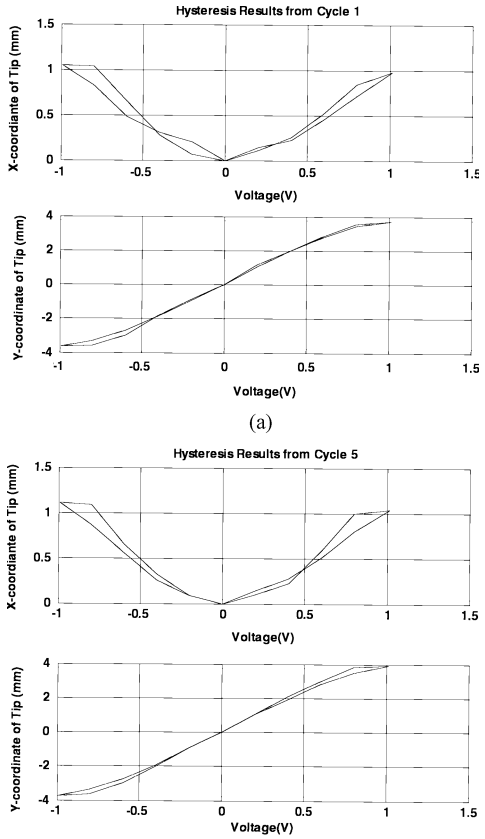

Fig. 19. X and Y displacements of the robotic finger under a ± 1 V cyclic triangle input. (a) Cycle 1. (b) Cycle 5.

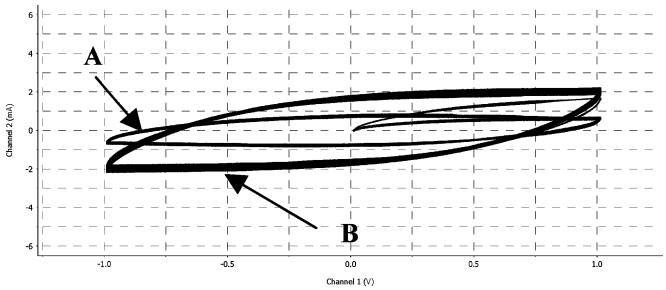

Fig. 20. The voltammetry diagram for the robotic finger under a ± 1 V cyclic triangle input; for the first 5 cycles (A), and for the first 40 cycles (B).

of the robotic finger is defined by X, Y coordinates of the tip as shown in Fig. 3. The X, Y coordinates of the tip displacement are provided in Fig. 19, where the hyteresis is not significant. The output current versus the input voltage curve, known as a voltammetry diagram, which is recorded for the same sample to further verify whether the hysteresis is significant, is shown in Fig. 20. The upper and lower portions of the voltammetry diagram are known as the oxidation and reduction curves, respectively. If the curves are symmetrical about the horizontal zero axis, this will indicate no hysteresis [25]. The symmetry is evident in the curves in Fig. 20, which supports the results provided in Fig. 19. When compared to the hysteresis results presented in the literature for a bilayer polymer actuator operating

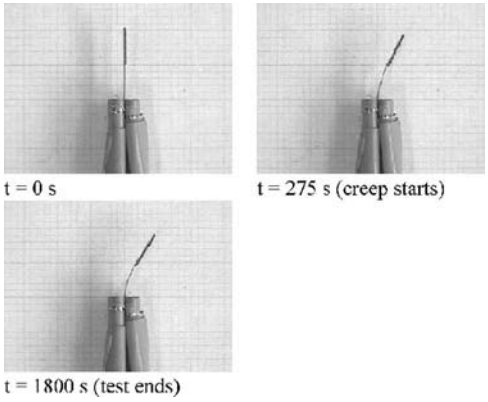

Fig. 21. Photographs of the robotic finger showing the creep starting instant and the end of creep test for the input voltage of 0.6 V.

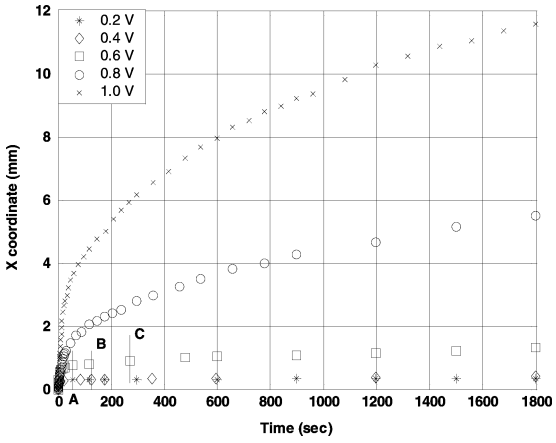

Fig. 22. X coordinate of the tip displacement versus time. The creep starts at A, B, and C for input voltages of 0.2, 0.4, and 0.6 V, respectively.

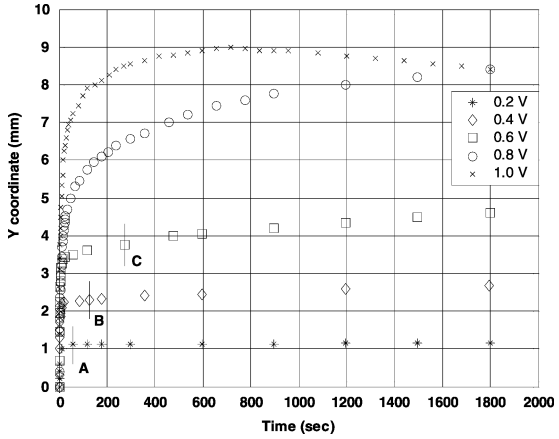

Fig. 23. Y coordinate of the tip displacement versus time. The creep starts at A, B, and C for input voltages of 0.2, 0.4, and 0.6 V, respectively.

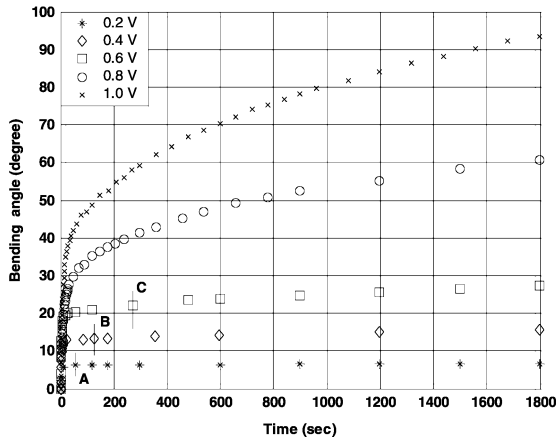

Fig. 24. Bending angle θ versus time. The creep starts at A, B, and C for input voltages of 0.2, 0.4, and 0.6 V, respectively.

in an aqueous medium [7], in which the hysteresis was reported to be 27° bending angle, the hysteresis in our trilayer actuator is negligibly small. We believe that the reason why our trilayer actuator shows virtually no hysteresis behavior may have been due to its symmetrical structure. The reason(s) need to be thoroughly investigated.

To evaluate the hysteresis repeatability of the actuator, a voltammetry diagram for 40 cycles, the curves indicated by "B" was also obtained and presented in Fig. 20, where it is obvious that the repeatability of the actuator is acceptable.

B. Creep Evaluation for the Robotic Finger

We describe the creep behavior in the conducting polymer actuator as the change in the tip position of the actuator after the polymer layers are fully oxidized, i.e., a zero-current output is recorded from the oxidized polymer layer. The creep observed for a 0.6 V input is presented in Fig. 21. With reference to the coordinate frame described in Fig. 3, the tip positions are identified as the robotic finger continuously bends under the effect of the step input voltages ranging from 0.2 to 1.0 V. The variation of the tip coordinates X, Y and the bending angle θ with time are depicted in Figs. 22–24.

The vertical lines across the response curves of 0.2, 0.4, and 0.6 in Figs. 22–24 indicate the instant when the creep starts. The zero current could not be recorded during the experiment period for the input voltages of 0.8 and 1.0 V, and hence, the creep response in these cases could not be fully recorded. When the experimental creep results of our trilayer actuator operating in air is compared to the experimental findings reported for a trilayer polymer actuator (20 mm $\times$ 15 mm $\times$ 0.013 mm) operating in a 1-M $LiClO_4$ aqueous solution [26], our actuator shows a nonnegligible creep behavior as opposed to the results provided in [26]. With reference to Fig. 24, when a zero current was recorded for a constant 0.6 V after 272.5 s, the bending angle was measured to be 21.96°.

However, after 1797.5 s the bending angle measured was 27.33°. This follows that the final position of the actuator did not stay fixed under a zero current.

C. Viscoelastic Model for Creep Behavior of the Robotic Finger

The low-frequency creep response of the robotic finger can be represented by a system of spring and damper elements, known as Kelvin–Voigt viscoeleastic model shown in Fig. 25.

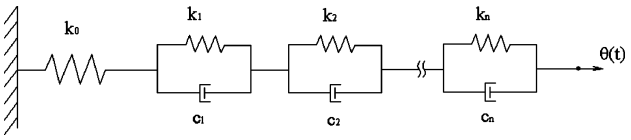

Fig. 25. Kelvin–Voigt model for viscoelastic materials.

TABLE I
RMS ESTIMATION ERRORS BETWEEN THE THEORETICAL AND EXPERIMENTAL RESULTS

Model	0.2 V	0.4 V	0.6 V	0.8 V	1.0 V
1	0.2154	0.7394	1.9318	5.1842	56.6855
2	0.0483	0.5415	0.3004	1.1743	1.4814
3	0.0479	0.1227	0.2078	0.4380	0.6268
4	0.2154	0.1222	0.1663	0.2081	0.2199
5	0.2154	0.1221	1.9318	0.1756	0.2057

This model was originally proposed to mimic the viscoeleastic behavior of polymers [27], and later used to predict the creep behavior of piezoactuators [28], [29].

The transfer function representation of this model is given by

$$\frac{\theta(t)}{u(t)} = \frac{1}{k_{x_0}} + \sum_{i=1}^{n} \frac{1}{k_i}\left[1 - e^{-k_i t/c_i}\right] \tag{8}$$

where $\theta(t)$ and $u(t)$ are the bending angle and the input voltage, respectively. The first term on the right-hand side represents elastic behavior while the second term, which represents Kelvin–Voigt elements, models creep behavior. The more the Kelvin–Voigt elements used in the model, the smaller are the errors between the estimated and the experimental data points. The accuracy of the model is evaluated using the root mean square (RMS) error (shown in Table I for various numbers of Kelvin–Voigt elements), which is given by

$$RMS_{bending\ angle} = \sqrt{\frac{1}{N}\sum_{i=1}^{N}(\theta_m - \theta_e)_i^2}. \tag{9}$$

The numerical values of the spring and damping parameters in (8) have been estimated for the input voltages of 0.2, 0.4, 0.6, 0.8, and 1.0 V using a least-square estimation algorithm. The estimated and experimental bending angle results are shown in Fig. 26.

The creep behavior of the finger operating in the vertical plane has also been evaluated to be quite similar. This follows that the rigid carbon fiber, which is treated as the uniformly distributed load at the tip of the actuator, does not have much influence on the creep behavior. The mechanism behind the creep behavior is mainly due to the osmotic pressure in the oxidized PPy layer, which is highly populated with the PF_6^- ions and solvent molecules, with reference to (1). Under osmotic pressure, the ions and molecules cannot go back to the other PPy layer as the input potential is still applied. Hence, they tend to spread around under the pressure, which results in further bending of the fully reduced PPy layer, and hence causing creep. This explanation is in agreement with the postulated explanation reported in the literature by Baughman [9] that the creep could be due to "electrical self-discharge or intraelectrode dopant redistribution after a fast mechanical response." In fact, the creep effect is more apparent with 0.6 V than with 0.2 V or 0.4 V, as seen in Fig. 26. Future work involves using an ionic electrolyte with larger molecule diameter and different dopant concentrations such that the cations and solvent molecules do not spread around much. Our initial experimental results, which will be reported in another publication, support this explanation.

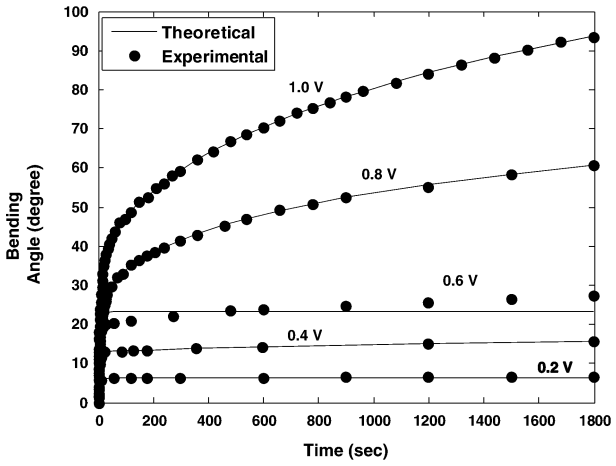

Fig. 26. Experimental and theoretical bending angle results for the finger operating in the horizontal plane.

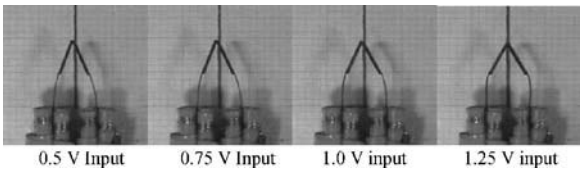

Fig. 27. Operation of the two fingers under different input voltages. The results are obtained 5 min after the voltages are applied.

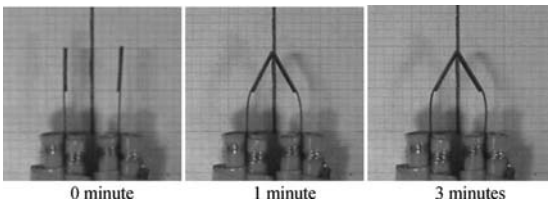

Fig. 28. Operation of the fingers for a driving voltage of 1.25 V at different instants.

D. Experimental Results

The gripper was first set up to operate in the horizontal plane to demonstrate the coordination of the two fingers. Fig. 27 shows the meeting points of two finger tips of the gripper under input voltages of 0.5, 0.75, 1.0, and 1.25 V. Except for 1.25-V input, the meeting points in three other cases of driving voltages do not lie on the middle line of the gripper. For a driving voltage of 1.25 V, two finger tips first met each other outside the middle line. However, it was observed that one finger was pushing the other such that the meeting point was lying on the middle line after 3 min, as depicted in Fig. 28.

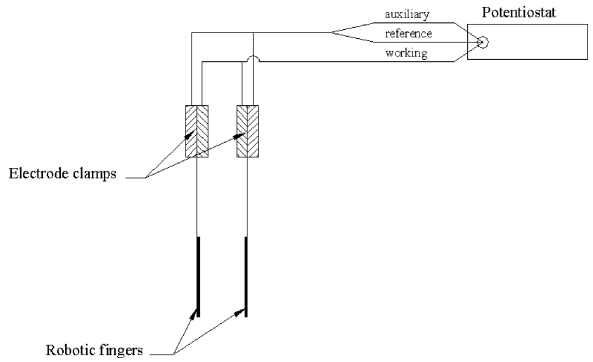

Fig. 29. Connection of the gripper electrodes to the eDAQ Potentiostat.

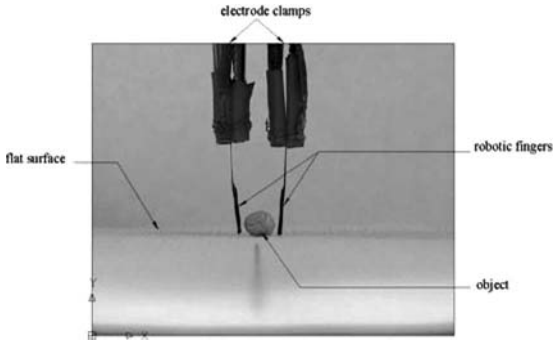

Fig. 30. Gripper configuration.

VII. Microgripping System

Two of the robotic fingers are assembled to make a robotic gripper, which is connected to the eDAQ Potentiostat as shown in Fig. 29. The gripper is arranged to operate in the vertical plane and grasp an object on a flat surface, as shown in Fig. 30.

We conducted a set of experiments under step voltages of 0.5, 0.75, 1.0, 1.25, and 1.5 V to quantify the load-carrying capability of the gripper. For each input voltage, the maximum load and the payload that the gripper can carry is identified. The variation of payload-to-gripper-mass ratio with the input voltage is shown in Fig. 31. The higher is the input voltage, the heavier is the load that the gripper can carry. The gripper can carry as much as 50 times more than its mass under a voltage of 1.5 V. We define the payload-to-weight ratio by W_O/W_G, where W_O is the load carried by the gripper, and W_G is the weight of the gripper itself. For the gripper considered, the total mass of the actuator parts and the rigid parts are 1.94 and 4.9 mg, respectively.

With reference to Fig. 32

$$2F_f = W_O, \quad 2\mu F_{\text{finger}} = W_O, \Rightarrow \mu = \frac{W_O}{2F_{\text{finger}}} \tag{10}$$

where F_{finger} is the force generated at the tip of the finger. The experimental F_{finger} results provided in the bottom plot of Fig. 15 can be used to estimate the friction coefficient μ. The weight W_O of the object can be interpolated from the experimental data as shown in Fig. 31. Substituting the corresponding values of F_{finger} and W_O into (10) gives the estimated values of μ, which have relatively small variations with the applied voltage, as shown in the bottom plot of Fig. 31. The average value of μ can be used to predict the weight to be carried by the gripper under different input voltages using (10). From the maximum loads the gripper can handle without any slippage, the friction coefficient between the object surface, which is industrial type

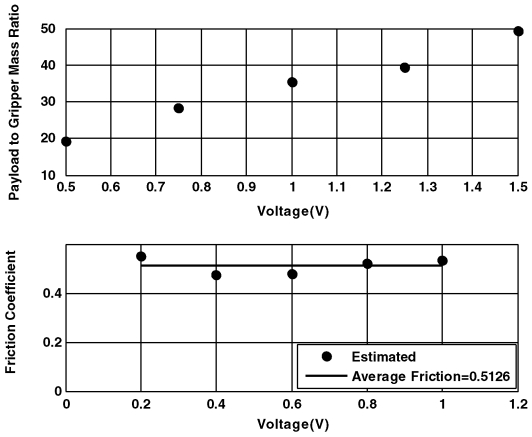

Fig. 31. Payload-to-gripper mass ratio versus input voltage (*top plot*), and estimated friction coefficient μ (*bottom plot*). The solid line shows the average value 0.5126 of μ.

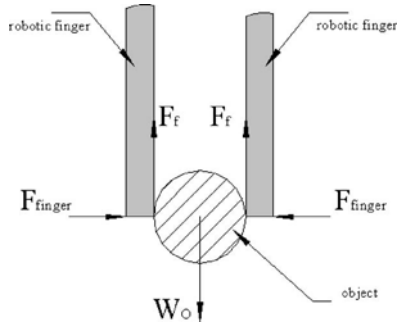

Fig. 32. Gripper handling a spherical object.

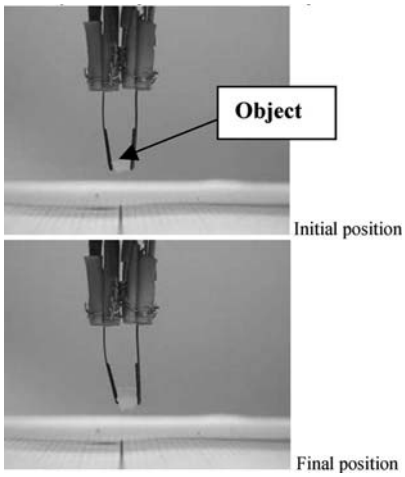

Fig. 33. Demonstration of the gripper ability to move an object within a small distance.

tissue paper, and the carbon fiber used to make the rigid part of each finger can be estimated.

The ability of the gripper to transport an object within a small distance is also demonstrated. While the gripper was holding the object, one of its fingers was disconnected from the potentiostat. The electrodes of that finger were short-circuited to bring the finger back to its neutral position. In the mean time, the potential is still applied to the other finger, which pushes the disconnected finger. The overall effect is to move the object sideways toward the disconnected finger, as shown in Fig. 33. The input voltage was a step voltage of 0.75 V, and the object weight was about 8 mg.

VIII. Conclusion

In this paper, we have presented new experimental and theoretical results demonstrating that conducting polymer actuators have many positive features, which allow them to be used in making functional robotic devices. We developed and experimentally verified a force output model for a trilayer PPy-type polymer actuator, and extended this model to estimate the force at the tip of a rigid link carried by the actuator. We quantified the nonlinear behavior, i.e., the hysteresis and creep behavior of the actuator driving a load in order to develop a nonlinear compensation strategy to improve the positioning accuracy of the actuator. The experimental results prove that the creep can cause significant positioning accuracy, if it is not properly identified and compensated. The hysteresis effect is found to be negligibly small—which requires further research work in order to completely explain it. As polymers exhibit viscoelastic behavior, Kelvin–Voigt creep model is employed to mimic the creep behavior. Immediate future study includes developing and implementing a motion/position control system, which adjusts the voltage applied to compensate for positioning the inaccuracy. As part of this aim, Kelvin–Voigt model should also be modified/improved to predict the creep behavior of a loaded actuator as a function of both time and input voltage. The performance of the microgripping system made up of two fingers articulated with the actuators is quantified in terms of payload handling and accurate positioning. Based on the maximum mass that the gripper can carry, the friction coefficient between the gripper surface and the object surface are experimentally determined, which is employed to determine the gripper force. Future work involves: 1) microfabricating the polymer actuator and the rigid link, and build more complicated functional devices and 2) using the viscoeleastic model or sensory position feedback based on laser displacement measurement to compensate for the creep.

Acknowledgment

The authors would like to thank Prof. G. M. Spinks, and Y. Wu from the Intelligent Polymer Research Institute for providing the actuators, allowing the use of some of their research facilities, and more importantly sharing their sterling expertise.

References

[1] E. W. H. Jager, E. Smela, O. Inganas, and I. Lundstrom, "Polypyrrole microactuators," *Synth. Met.*, pp. 1309–1310, 1999.

[2] G. M. Spinks, B. Xi, D. Zhou, V. T. Truong, and G. G. Wallace, "Enhanced control and stability of polypyrrole electromechanical actuators," *Synth. Met.*, vol. 140, pp. 273–280, 2004.

[3] J. Ding, L. Liu, G. M. Spinks, D. Zhou, V. T. Truong, G. G. Wallace, and J. Gillespie, "High performance conducting polymer actuators utilising a tubular geometry and helical wire interconnects," *Synth. Met.*, vol. 138, pp. 391–398, 2002.

[4] J. W. L. Zhou, H. Y. Chan, T. K. H. To, K. W. C. Lai, and W. L. Li, "Polymer MEMS actuators for underwater micromanipulation," *IEEE/ASME Trans. Mechatronics*, vol. 9, no. 2, pp. 334–342, Jun. 2004.

[5] J. D. Madden, R. A. Cush, T. S. Kanigan, and I. W. Hunter, "Fast contracting polypyrrole actuators," *Synth. Met.*, vol. 113, pp. 185–192, 2000.

[6] E. Smela, "Conjugated polymer actuators for biomedical applications," *Adv. Mat.*, vol. 15, no. 6, pp. 481–494, Mar. 2003.

[7] E. Smela, M. Kallenbach, and J. Holdenried, "Electrochemically driven polypyrrole bilayers for moving and positioning bulk micromachined silicon plates," *IEEE/ASME Trans. Microelectromech. Syst.*, vol. 8, no. 4, pp. 373–383, Dec. 1999.

[8] Q. Pei and O. Inganas, "Electrochemical applications of the bending beam method: 1. Mass transport and volume changes in polypyrrole during redox," *J. Phys. Chem.*, vol. 96, no. 25, pp. 10507–10514, 1992.

[9] R. H. Baughman, "Conducting polymer artificial muscles," *Synth. Met.*, vol. 78, pp. 339–353, 1996.

[10] G. G. Wallace, G. M. Spinks, L. A. P. Kane Maguire, and P. R. Teasdale, *Conductive Electroactive Polymers, Intelligent Materials Systems*, 2nd ed. Boca Raton, FL: CRC Press, 2003.

[11] L. Bay, T. Jacobsen, S. Skaarup, and K. West, "Mechanism of actuation in conducting polymers: Osmotic expansion," *J. Phys. Chem. B*, vol. 105, pp. 8492–8497, 2001.

[12] T. F. Otero and M. T. Cortes, "Artificial muscle: Movement and position control," *Chem. Commun.*, pp. 284–285, 2004.

[13] E. W. H. Jager, O. Inganas, and I. Lunstrom, "Microrobots for micrometer-size objects in aqueous media: Potential tools for single cell manipulation," *Science*, vol. 288, pp. 2335–2338, Jun. 30, 2000.

[14] J. W. L. Zhou and W. L. Li, "Micro ICPF actuators for aqueous sensing and manipulation," *Sens. Actuators A*, vol. 114, pp. 406–412, 2004.

[15] G. Alici and B. Shirinzadeh, "Kinematics and stiffness analysis of a flexure-jointed planar micromanipulation system for a decoupled compliant motion," in *Proc. IEEE/RSJ Int. Conf. Intell. Robots Syst.*, vol. 4, Las Vegas, NV, Oct. 27–31, 2003, pp. 3282–3287.

[16] G. Alici, B. Mui, and C. Cook, "Bending modeling and its experimental verification for conducting polymer actuators dedicated to manipulation applications," *Sens. Actuators A*, vol. 126, no. 2, pp. 396–404, Feb. 14, 2006.

[17] G. Alici, P. Metz, and G. M. Spinks, "A mathematical model to describe bending mechanics of polypyrrole (PPy) actuators," in *Proc. 2005 IEEE/ASME Int. Conf. Adv. Intell. Mechatronics*, Monterey, CA, pp. 1029–1034.

[18] S. W. John and G. Alici, "Towards micro and nano manipulation systems: Behaviour of a laminated polypyrrole (PPy) actuator driving a rigid link," in *Proc. 2005 IEEE/ASME Int. Conf. Adv. Intell. Mechatronics*, Monterey, CA, pp. 54–59.

[19] G. Alici and N. N. Huynh, "Predicting force output of trilayer polymer actuators," *Sens. Actuators A*, vol. 132, no. 2, pp. 616–625, Nov. 2006.

[20] G. Alici, P. Metz, and G. M. Spinks, "A methodology towards geometry optimisation of high performance polypyrrole (PPy) actuators," *J. Smart Mat. Struct.*, vol. 15, pp. 243–252, 2006.

[21] B. S. Berry and W. C. Pritchet, "Bending cantilever method for the study of moisture swelling in polymers," *IBM J. Res. Develop.*, vol. 28, no. 6, 1984.

[22] S. Timoshenko, "Analysis of bi-metal thermostat," *J. Opt. Soc. Amer.*, vol. 11, p. 233, 1925.

[23] J. D. W. Madden, P. G. A. Madden, and I. W. Hunter, "Polypyrrole actuators: Modeling and performance," *Proc. SPIE-Smart Struct. Mat. Electroactive Polymer Actuators Dev.*, vol. 4329, pp. 72–83, 2001.

[24] Y. Wu, G. Alici, G. M. Spinks, and G. G. Wallace, "Fast tri layer polypyrrole bending actuators for high speed applications," *Synth. Met.*, vol. 156, no. 16/17, pp. 1017–1022, Aug. 2006.

[25] G. Grande and T. F. Otero, "Intrinsic asymmetry, hysteresis, and conformational relaxation during redox switching in polypyrrole: A coulovoltametric study," *J. Phys. Chem.*, vol. 102, pp. 7535–7540, 1998.

[26] T. F. Otero and M. T. Cortes, "Characterisation of triple layers," *Proc. SPIE-Smart Struct. Mat. Electroactive Polymer Actuators Dev.*, vol. 4329, pp. 93–100, 2001.
[27] L. E. Malvern, *Introduction to the Mechanics of a Continuous Medium*. Englewood Cliffs, NJ: Prentice-Hall, 1969.
[28] D. Croft, G. Shed, and S. Devasia, "Creep, hysteresis, and vibration compensation for piezoactuators: Atomic force microscopy application," *J. Dyn. Syst., Meas., Control*, vol. 123, pp. 35–43, 2001.
[29] R. Changhai and S. Lining, "Hysteresis and creep compensation for piezoelectric actuator in open-loop operation," *Sens. Actuators A*, vol. 122, pp. 124–130, 2005.

Gursel Alici received the B.Sc. degree (with high honors) from the Middle East Technical University, Gaziantep, Turkey, in 1988, and the M.Sc. degree from Gaziantep University, Gaziantep, Turkey, in 1990 in mechanical engineering, and the Ph.D. degree in robotics from Oxford University, Oxford, U.K., in 1993.

He is currently an Associate Professor with the School of Mechanical, Materials and Mechatronic Engineering at the University of Wollongong, NSW, Australia. His current research interests include mechanics, optimum design, control, and calibration of mechanisms/robot manipulators/parallel manipulators, micro/nano manipulation systems, and modeling, analysis, and characterisation of conducting polymer actuators and sensors for use in functional robotic devices. He has authored or coauthored more than 100 papers published in international journals and conference proceedings.

Nam N. Huynh received the B.E. degree in aeronautical engineering from the Vietnam National University, Hochiminh City, Vietnam, in 2004. He received the M.E. degree in mechatronic engineering in 2005 with a thesis on performance evaluation of a conducting polymer-based gripping system from the University of Wollongong, NSW, Australia, where he is currently working toward the Ph.D. degree in mechanical engineering.